Using an iterative eigensolver and intertwined rank reduction to compute vibrational spectra of molecules with more than a dozen atoms: uracil and naphthalene

Phillip S. Thomas

e-mail: Phillip.Thomas@chem.queensu.ca

Tucker Carrington Jr.

e-mail: Tucker.Carrington@queensu.ca

fax: 613-533-6669

Chemistry Department, Queen's University

Kingston, Ontario, Canada

K7L 3N6

Canada

Jay Agarwal

Henry F. Schaefer III

Center for Computational Chemistry, University of Georgia

Athens, Georgia 30602-0525

10/02/2017

Abstract

We use a direct product basis, basis vectors computed by evaluating matrix-vector products, and rank reduction to calculate vibrational energy levels of uracil and naphthalene, with 12 and 18 atoms, respectively. A matrix representing the Hamiltonian in the direct product basis and vectors with as many components as there are direct product basis functions are neither calculated nor

stored. We also introduce an improvement of the Hierarchical Intertwined Reduced-Rank Block Power Method (HI-RRBPM), proposed previously in J. Chem. Phys, 146, (2017), 204110. It decreases the memory cost of the HI-RRBPM and enables one to compute vibrational spectra of molecules with over a dozen atoms with a typical desktop computer.

I. Introduction

In this paper we report variational calculations of vibrational energy levels of uracil and naphthalene, having 12 and 18 atoms. For molecules of this size, it is more common to use perturbation theory.[1] Unlike perturbation theory, variational calculations systematically account for the effects of strong coupling and nearly degenerate states. To do the variational calculations we use a direct product basis. A direct product basis has the important advantage of simplicity, but its size scales exponentially with the number of atoms.[2–4] The memory and computer time required to compute a spectrum can be significantly reduced by using iterative eigensolvers.[5–9] They require only enough memory to store several vectors. However, for molecules with more than four atoms even the amount of memory required to store direct-product basis vectors is excessive. In this paper, although we use a direct product basis, elements of a matrix representing the Hamiltonian in the direct product basis and vectors with as many components as there are direct product basis functions are neither calculated nor stored.

The method we use works only if the potential energy surface (PES) is a sum of products (SOP). For molecules with fewer than about 5 or 6 atoms, it is possible to construct accurate PESs that often are not SOPs.[10,11] For such molecules, quadrature or collocation is essential.[4,12–19] For larger molecules, the best available PESs are often SOPs. When the PES is a SOP and each basis function is a product of univariate factors, the calculation of its matrix elements is inexpensive because they can be assembled from sums of products of 1D integrals. Although this greatly simplifies the calculation, one must still develop tools that make it possible to compute eigenvalues of the (implicit) Hamiltonian matrix.

If the PES is a SOP, one way to compute a spectrum is to use a basis whose functions are

products of univariate functions, but which is not a full direct product basis. Such a basis is often obtained by pruning.[20–27] Using mapping techniques[26,28,29] or well known algorithms for storing sparse matrices,[27,30] it is possible to evaluate the matrix-vector products (MVPs) required to use an iterative eigensolver.

In this paper we use different ideas.[31,32] In Ref. 31, Leclerc and Carrington used SOP basis functions, basis vectors generated by evaluating matrix-vector products, and rank reduction with an alternating least squares algorithmx.[33] The SOP basis functions are not functions selected from a direct product basis. Each basis function has the form,

$$\Psi\left(q_1,\ldots,q_D\right) \simeq \sum_{i_1=1}^{n_1} \cdots \sum_{i_D=1}^{n_D} F_{i_1,\ldots,i_D} \prod_{c=1}^{D} \varphi_{i_c}^{c}\left(q_c\right) \ , \tag{1}$$

where $\varphi_{i_c}^{c}\left(q_c\right)$ are 1-D basis functions depending on coordinate q_c, and

$$F_{i_1,\ldots,i_D} = \sum_{r=1}^{R_\psi} s_r^{\mathbf{F}} \prod_{c=1}^{D} f_{i_c}^{(r,c)} \ , \tag{2}$$

is a tensor of basis coefficients. In Eq. 2, $f^{(r,c)}$ is a 1-D vector of coefficients and $s_r^{\mathbf{F}}$ is a normalization factor. A basis vector expressed as in eq 2 is said to be in CP-format.[34] The number of terms, R_ψ, is referred to as the rank. To store $F_{i_1,\ldots,i_D}$, one needs only to store the $f_{i_c}^{(r,c)}$, which requires storing RnD numbers, where n is a representative value of $n_1, n_2, \cdots, n_D$ and D is the number of degrees of freedom. The number of terms in each of the basis vectors is reduced as they are computed. These ideas were originally implemented in the Reduced Rank Block Power Method (RRBPM).[31] It uses CP format, a block-power method to generate basis vectors, and projects into the space spanned by CP vectors to compute eigenvalues. The key advantage of CP format is that the memory cost scales linearly in D (in constrast, when direct-product vectors are stored the memory cost scales as n^D). Mathematicians often shun CP format because algorithms for representing a tensor in CP format may converge poorly. As our goal is only to make basis vectors in CP format, we can compute exact eigenvalues even if reduction to CP format is imperfect. In previous calculations, we have demonstrated that good results can be obtained with small ranks

($R_\psi < 1000$).[31,32,35–37]

Other groups are also using related tensor methods. By far the most prominent is the multi-configuration time-dependent Hartree (MCTDH) method.[38,39] It uses tensors in what is called Tucker format.[34,40] When the tensor of coefficients is in Tucker format, wavefunctions are represented in an optimised direct product basis. To reduce the size of the MCTDH coefficient vectors one uses mode combination,[39] multiple layers,[41–43] and pruning.[44–47] Several years ago, it was observed that cluster amplitudes in a vibrational coupled cluster calculation could be stored in CP format.[48] More recently, it has been shown that it is possible to develop a vibrational coupled cluster method that not only stores but also calculates cluster amplitudes in CP format.[49] This new method has some of the same advantages of the RRBPM. A method like the RRBPM, but in which the vectors are generated with inverse iteration and vectors are represented in tensor train (or matrix product state) format is more efficient than the original RRBPM for acetonitrile.[50] The density matrix renormalized group (DMRG) method is often used by quantum chemists to calculate the ground state of the electronic Schroedinger equation.[51,52] It imposes the matrix product state (or tensor train) form on the ground state wavefunction and then optimizes it. The RRBPM optimises not a wavefunction, but basis functions and then computes eigenstates by solving a (small) generalized eigenvalue problem. In Ref. 53, energy levels of the helium atom are computed using basis vectors in CP format by building a basis from matrix-vector products (MVPs). The start vectors of the block are chosen to be eigenstates of a separable Hamiltonian; the iterative eigensolver is different and the updating or restarting is also different than in Refs. 31,32,35

Most variational calculations are memory bound, i.e., it is the amount of memory available that determines whether or not a calculation is possible. The strategy of using MVPs to make basis functions that are stored in a tensor format eliminates the memory problem. With the RRBPM it is possible to compute the lowest 70 eigenstates of CH_3CN using less than 1 GB of memory.[31] Even for larger molecules, not much memory is required.[32,35,37] There are, however, other problems: (1) for molecules with more than seven atoms, the RRBPM converges slowly, requiring > 1000 matrix-vector products (MVPs) per desired state to achieve modest accuracy; (2) calculations take a lot of computer time because of the need to reduce the number of terms in the SOP basis vectors

(rank reduction).

Convergence can be improved in several ways, including performing separate calculations for different symmetries,[36] using an eigensolver with a better convergence rate than the shifted power method,[37,54] and by grouping coordinates of the molecule into a tree structure and constructing the basis hierarchically by solving eigenproblems for subsets of the coordinates.[35] The Hierarchical (H-) RRBPM adopts this last strategy. It uses the RRBPM to compute eigenstates at each node of the tree. With a good choice of tree, the H-RRBPM is orders-of-magnitude faster than the ordinary RRBPM. At each node of the tree, the spectrum of the reduced-dimensional eigenproblem is less dense than that of the full-dimensional eigenproblem, and thus applying the RRBPM node-wise results in faster convergence than applying the RRBPM to the full-dimensional problem. Many papers use bases composed of eigenfunctions of reduced dimension Hamiltonians for subsets of the coordinates.[55–57] When using the H-RRBPM, nodes in the tree are treated sequentially. In contrast, Multi-layer MCTDH treats all of the nodes simultaneously.

The most costly ($> 90\%$) part of an RRBPM calculation is the reduction of the rank of the basis vectors, which is increased when a MVP is performed or when the basis is orthogonalized/updated. The original RRBPM used an Alternating Least Squares (ALS) algorithm[58] to reduce the ranks. Recently, we proposed a method which "intertwines" evaluation of MVPs with rank reduction.[32] In the intertwined (I-) RRBPM, there is a partial rather than a full optimization of a vector after each MVP. It is approximately an order of magnitude faster than the original RRBPM. The faster optimization makes it practical to use larger ranks, which in turn allows one to compute vibrational energy levels for larger molecules or for smaller molecules with higher precision, despite the fact that the optimizations are less good. We demonstrated that using intertwining with the H-RRBPM it is possible to compute vibrational energy levels for an 11-atom molecule such as cyclopentadiene (C_5H_6). Moreover, the I-RRBPM can be formulated to avoid storing the large-rank vectors which are created after matrix-vector products and orthogonalization/updates, reducing the memory cost.

In this paper we propose a slightly modified version of the I-RRBPM which further reduces its memory cost. We call it the "ultra-low-memory" I-RRBPM. It will make it possible to use the I-RRBPM with graphical processing units (GPUs). We also compute energy levels of two molecules,

uracil ($C_4H_4O_2N_2$) with 12 atoms and naphthalene ($C_{10}H_8$) with 18 atoms, using the HI-RRBPM. The modification is introduced to decrease the memory required to store matrices of inner products which are used for rank-reduction in the I-RRBPM. They become large (for naphthalene they require hundreds of GB) when the number of terms in the Hamiltonian or the number of vectors computed in parallel is large. Although many modern computers have hundreds of GB of memory, we would like to have a method for doing variational calculations on molecules like naphthalene on a standard desktop computer.

II. Theory

A. Computing vibrational energy levels using vectors in CP-format

The basic strategy is to make a set of CP vectors and to project into the space they span to compute eigenvalues. To convert this strategy into a computational method we must specify how the CP vectors are calculated. In the RRBPM, a block of vectors is evolved by evaluating MVPs. If a vector is in CP format then the vector obtained from it by applying a shifted SOP Hamiltonian to it is also in CP format. We write the SOP Hamiltonian as

$$\hat{H} = \sum_{m=1}^{T} \prod_{c=1}^{D} \hat{h}_{m,c} , \tag{3}$$

where $\hat{h}_{m,c}$ is an operator depending only on coordinate c. A matrix-vector product (MVP) is[31]

$$\begin{aligned}
(\mathbf{G})_{i'_1,i'_2,\ldots i'_D} &= (\mathbf{HF})_{i'_1,i'_2,\ldots i'_D} \\
&= \sum_{i_1,i_2,\ldots i_D} \left(\sum_{m=1}^{T} \prod_{c'=1}^{D} \hat{h}_{m,c'} \right)_{i'_1,i'_2,\ldots i'_D,i_1,i_2,\ldots i_D} \sum_{r=1}^{R_\psi} s_r \prod_{c=1}^{D} f_{i_c}^{(r,c)} \\
&= \sum_{m=1}^{T} \sum_{r=1}^{R_\psi} s_r \prod_{c=1}^{D} \sum_{i_c} \left(\hat{h}_{m,c} \right)_{i'_c,i_c} f_{i_c}^{(r,c)} \\
&= \sum_{m=1}^{T} \sum_{r=1}^{R_\psi} s_r \prod_{c=1}^{D} g_{i'_c}^{(r,c)} \\
&= \sum_{r'=1}^{R_G} s_{r'}^{G} \prod_{c=1}^{D} g_{i'_c}^{(r',c)} \, . \qquad (4)
\end{aligned}$$

Although $(\mathbf{G})_{i'_1,i'_2,\ldots i'_D}$ in Eq. (3) is a CP vector, it is a CP vector with a much larger rank. The MVP produces a vector which has T times as many terms as $\mathbf{F}$. We denote all large-rank vectors $\mathbf{G}$ (rank $\gg R_\psi$) and small-rank vectors $\mathbf{F}$ (rank$= R_\psi$). Because many MVPs are required, it is necessary to reduce the rank of $\mathbf{G}$ after each MVP to keep the memory cost low. This means finding a vector, ${}^{out}\mathbf{F}$, which minimizes $\|{}^{out}\mathbf{F} - \mathbf{G}\|$. In the original RRBPM, we used an Alternating Least Squares (ALS) method[58] to compute ${}^{out}\mathbf{F}$, unless there are only two coordinates, in which case we used Singular Value Decomposition (SVD).[59] ${}^{out}\mathbf{F}$ then replaces $\mathbf{F}$ and another MVP is evaluated.

The ALS procedure cycles through coordinates $c = 1 \ldots D$ and computes an improved set of $\boldsymbol{f}^{(r,c)}$ for each value of c. For each coordinate, one computes matrices of inner products, defined

as:

$$B^c_{r',r} = \left\langle \boldsymbol{f}^{(r',c)}, \boldsymbol{f}^{(r,c)} \right\rangle \tag{5a}$$

$$P^c_{r',r} = \left\langle \boldsymbol{g}^{(r',c)}, \boldsymbol{f}^{(r,c)} \right\rangle \tag{5b}$$

$$B^{\neq c}_{r',r} = \prod_{c' \neq c} B^{c'}_{r',r} \tag{5c}$$

$$P^{\neq c}_{r',r} = \prod_{c' \neq c} P^{c'}_{r',r} \tag{5d}$$

$$B_{r',r} = \prod_{c=1}^{D} B^c_{r',r} \tag{5e}$$

$$P_{r',r} = \prod_{c=1}^{D} P^c_{r',r}, \tag{5f}$$

where coordinate c is *omitted* from $\boldsymbol{B}^{\neq c}$ and $\boldsymbol{P}^{\neq c}$. $\boldsymbol{P}^{\neq c}$ is used to construct right-hand sides of sets of linear systems,

$$b^{(i_c,c)}_r = \sum_{r'=1}^{R_{\mathbf{G}}} s^{\mathbf{G}}_{r'} \, g^{(r',c)}_{i_c} P^{\neq c}_{r',r} \, . \tag{6}$$

which are solved for $\boldsymbol{x}^{(i_c,c)}$:

$$\boldsymbol{B}^{\neq c} \boldsymbol{x}^{(i_c,c)} = \boldsymbol{b}^{(i_c,c)} \, . \tag{7}$$

The solutions $x^{(i_c,c)}_r$ replace $f^{(r,c)}_{i_c}$. Each $\boldsymbol{f}^{(r,c)}$ is then normalized so that $s^{\mathbf{F}}_r = \left\| \boldsymbol{f}^{(r,c)} \right\|$ and ${}^{normalized}\boldsymbol{f}^{(r,c)} = \frac{\boldsymbol{f}^{(r,c)}}{\left\| \boldsymbol{f}^{(r,c)} \right\|}$. Applying eqs 5a-7 to compute new $\boldsymbol{f}^{(r,c)}$ for coordinates $c = 1 \ldots D$ in sequence constitutes one ALS sweep.

The Reduced Rank Block Power Method (RRBPM)[31] repeatedly applies the following steps to a block of $\mathcal{B}$ basis vectors, $\mathcal{F} = \{\mathbf{F}_k\}$ ($k = 1 \ldots \mathcal{B}$): 1) matrix-vector product $\mathbf{G}_k = (\mathbf{H} - E_s 1)\,{}^{in}\mathbf{F}_k$, and 2) $\mathbf{G}_k \xrightarrow{ALS} {}^{out}\mathbf{F}_k$. After every N_{pow} MVP+ALS steps the $\mathcal{B}$ vectors are Gram-Schmidt orthogonalized and then used as a basis for solving a small $\mathcal{B} \times \mathcal{B}$ generalized eigenvalue problem.

The solution vectors then replace $\mathcal{F}$. This process (or *cycle*) is repeated until the set of vectors converges to the eigenvectors associated with the B smallest eigenvalues.

In the RRBPM, after each MVP, ALS is used to optimize $f^{(r,c)}$ for *all* $c = 1 \ldots D$. One sweep corresponds to optimizing $f^{(r,c)}$ for all the coordinates. Many sweeps constitute one application of the ALS method. In the "intertwined" (I-) RRBPM,[32] after each MVP, $f^{(r,c)}$ is optimized for a single coordinate. The other $f^{(r,c')}$, $c' \neq c$ in ${}^{out}\mathbf{F}$ are set equal to the values they had before the MVP was evaluated. This is therefore a partial and not a full optimization. It is equivalent to computing $g^{(r',c)} = h_{m,c} f^{(r,c)}$ (note that a value of r' is associated with values of both r and m) and then optimizing ${}^{out}f_{i_c}^{(r,c)}$ for *one* coordinate c at a time. For all $c' \neq c$, ${}^{out}f_{i_{c'}}^{(r,c')}$ are set to ${}^{out}f_{i_{c'}}^{(r,c')} = {}^{in}f_{i_{c'}}^{(r,c')}$. A loop over all coordinates $c = 1 \ldots D$ constitutes one sweep. In the original RRBPM, performing N_{pow} MVP+ALS steps requires one to construct and solve $N_{pow} N_{sweep} D$ linear systems, where N_{pow} and N_{sweep} have typical values of 10-20. In the I-RRBPM only $N_{sweep} D$ linear systems need to be constructed/solved per cycle. Moreover, in the RRBPM, the B and P matrices must be constructed "from scratch" for all $c = 1 \ldots D$ every time ALS is called. In contrast, in the I-RRBPM the B and P matrices are constructed for all c only after the first MVP; they are updated for only a single value of c after each subsequent MVP. Constructing the linear systems accounts for the majority of the CPU time in an RRBPM calculation, so intertwining the MVP and ALS steps reduces the calculation cost by roughly an order of magnitude.

The most obvious way to use both the RRBPM and the I-RRBPM requires storing large-rank G vectors. The rank of the G vectors obtained after evaluating MVPs is TR_ψ. The Gram-Schmidt orthogonalization step and the step of replacing the $\mathcal{F}$ basis with solutions of the generalized eigenvalue problem both also produce large-rank vectors, but with a maximum of BR_ψ terms. The memory cost of storing the large-rank vectors is significant, if many vectors are computed in parallel and if either 1) there are many terms in the Hamiltonian (T is large), or 2) there are many vectors in the block (B is large). The "low-memory" version of I-RRBPM[32] reduces the memory cost by obviating the need to store the G vectors. Instead, a column of the $P_{r',r}^{\neq c}$ matrix is made and Eq. (7) is evaluated by successively adding contributions from different $g^{(r',c)}$ and discarding them after they have been used. This avoids the need to store vectors with $TR_\psi nD$

(or $BR_\psi nD$) entries. However, the low-memory version incurs a slightly higher CPU cost since it must generate the $g^{(r',c)}$ on-the-fly *twice* per c per sweep, first to compute $P^c_{r',r}$ for the downdate $P^{\neq c}_{r',r} = P_{r',r}/P^c_{r',r}$, and then to compute a new $P^c_{r',r}$ for the update $P_{r',r} = P^{\neq c}_{r',r} \cdot P^c_{r',r}$. In contrast, the full-memory version must generate $g^{(r',c)}$only once per c per sweep.

B. "Ultra-low-memory" intertwining

In this subsection we explain that it is possible to further reduce the memory required to use the I-RRBPM. Although it is possible to use the low-memory I-RRBPM of Ref. 32 to do variational calculations on molecules with more than a dozen atoms (in the next section we present results for naphthalene), in order to use the RRBPM on a standard personal computer to do such calculations, changes in the algorithm are necessary. Moreover, reducing the memory cost of the method will make it possible to use it with GPUs and thereby reduce the time required to compute a spectrum.

Relative to the RRBPM and full-memory I-RRBPM, the low-memory I-RRBPM significantly reduces the memory cost. However, if many vectors are computed in parallel and either T or B is large, hundreds of GB are required. The low-memory version requires storing $\boldsymbol{P}$ matrices. They have TR^2_ψ and up to BR^2_ψ elements for the MVP and Gram-Schmidt/vector update steps, respectively. For the largest calculations in this paper, $T = 767$ and $R_\psi = 700$, so storing a single $\boldsymbol{P}$ matrix requires 2.8 GB. To compute 128 states in parallel (*vide infra*), 358 GB is needed to store all of $\boldsymbol{P}$ matrices simultaneously.

The key idea of the ultra-low memory method we propose in this section is to generate *both* the $\mathbf{G}$ vector *and* the $\boldsymbol{P}^{\neq c}$ matrix on-the-fly and only in small portions, discarding them immediately after use. It is described in Algorithms 1-2. Algorithm 2, which does MVPs, is similar to the low-memory version described in Algorithm 4 of Ref.[32] What distinguishes the ultra-low memory version is the way $B^{\neq c}_{r',r}$ and $b^{(i_c,c)}_r$ are computed. In the low-memory version they are obtained by storing $\boldsymbol{B}$ and $\boldsymbol{P}$ and downdating and updating to get $\boldsymbol{B}^{\neq c}$ and $\boldsymbol{P}^{\neq c}$ matrices for each α, c pair. In the ultra-low-memory version, to avoid storing $\boldsymbol{P}$ (TR^2_ψ elements), $\boldsymbol{P}^{\neq c}$ is constructed from scratch, but in blocks, for each α, c. This is done inside Algorithm 2, which generates an $R_\psi \times R_\psi$

block of $P^{\neq c}$ for each value of $m = 1 \ldots T$. The blocks are used to construct the right-hand-sides $b^{(i_c,c)}$ of a linear system and then discarded.

Because when we apply the *shifted* Hamiltonian, $(\mathbf{H} - E_*\mathbf{1})\,\mathbf{F}$, the energy shift is the *last* ($m = T$) term in Algorithm 2, the last $R_\psi \times R_\psi$ block of the $P^{\neq c}$ matrix is

$$\begin{aligned} P^{\neq c} &= \prod_{c' \neq c} \left\langle g^{(r',c)}, f^{(r,c)} \right\rangle \\ &= \prod_{c' \neq c} \left\langle \mathrm{I} f^{(r',c)}, f^{(r,c)} \right\rangle \\ &= \prod_{c' \neq c} \left\langle f^{(r',c)}, f^{(r,c)} \right\rangle \\ &= B^{\neq c}, \end{aligned} \tag{8}$$

so Algorithm 2 provides the $B^{\neq c}$ matrix at no additional cost as part of the $b^{(i_c,c)}$ computation.

Algorithm 1 Intertwined power method, ultra-low-memory version.

Input: vector in block, $\mathbf{F}$, with rank $R_\mathbf{F}$
Output: improved vector in block, $\mathbf{F}$, with rank $R_\mathbf{F}$
for $\alpha = 1 \ldots N_{sweep}$:

for $c = 1 \ldots D$: (Loop over coordinates)

a) Call Algorithm 2 to calculate $B^{\neq c}_{r',r}$ for all r', r; and $b^{(i_c,c)}_r$ for all i_c, r (Eq. 6)

b) solve linear system for $x^{(i_c,c)}$ (Eq. 7); replace $f^{(r,c)}_{i_c} \leftarrow x^{(i_c,c)}_r$ for all i_c, r

c) normalize $s^{\mathbf{F}}_r \leftarrow \left\| f^{(r,c)} \right\|$; $f^{(r,c)} \leftarrow \frac{f^{(r,c)}}{\left\| f^{(r,c)} \right\|}$ for all r;

normalize $\mathbf{F} \leftarrow \frac{\mathbf{F}}{\|\mathbf{F}\|}$

The CPU cost of Algorithms 1-2 is $\mathcal{O}\left(N_{sweep} D \left(T R_\psi n_c^2 D + T R_\psi^2 n_c D + R_\psi^3\right)\right)$. Here, $T R_\psi n_c^2 D$ is the cost of computing the MVPs in steps $\mathrm{I}-1-\mathrm{b}-\mathrm{i}$ and $\mathrm{I}-1-\mathrm{c}$, and $T R_\psi^2 n_c D$ is the sum of the cost of the inner product in $\mathrm{I}-1-\mathrm{b}-\mathrm{ii}$ and updating $b^{(i_c,c)}_r$ in $\mathrm{I}-1-\mathrm{d}$, in Algorithm 2. The R_ψ^3 term is the cost of solving the linear system in step b of Algorithm 1. This cost is approximately a factor of $D/3$ larger than the full- and low-memory versions of I-RRBPM which store $P^{\neq c}$.

Algorithm 2 Pseudo-code for computing B matrices and right-hand sides $b^{(i_c,c)}$ without generating a large-rank vector $\mathbf{G}$ or matrix P.

Input: CP-format vector, $\mathbf{F}$, with rank $R_{\mathbf{F}}$
Output: matrix $B^{\neq c}$; right-hand sides, $b^{(i_c,c)}$
Initialize $b_r^{(i_c,c)} \leftarrow 0$ for all i_c, r; $P_{r',r}^{\neq c} \leftarrow 0$ for all r
I) for $m = 1 \ldots T$:

1) for $l = 1 \ldots R_\psi$:

a) $r' \leftarrow (m-1)\,R_\psi + l$

b) for $c' = 1 \ldots c-1, c+1, \ldots D$:

i) $\boldsymbol{g}^{(r',c')} \leftarrow \boldsymbol{h}_{m,c'} \boldsymbol{f}^{(l,c')}$

ii) for $r = 1 \ldots R_\psi$:

$$P_{r',r}^{\neq c} \leftarrow P_{r',r}^{\neq c} \left\langle \boldsymbol{g}^{(r',c')}, \boldsymbol{f}^{(r,c')} \right\rangle$$

iii) discard $\boldsymbol{g}^{(r',c')}$

c) $\boldsymbol{g}^{(r',c)} \leftarrow \boldsymbol{h}_{m,c} \boldsymbol{f}^{(l,c)}$

d) for $r = 1 \ldots R_\psi$:

if $m < T$: $b_r^{(i_c,c)} \leftarrow b_r^{(i_c,c)} + s_l^{\mathbf{F}} g_{i_c}^{(r',c)} P_{r',r}^{\neq c}$ for all i_c

else: $b_r^{(i_c,c)} \leftarrow b_r^{(i_c,c)} - E_s s_l^{\mathbf{F}} g_{i_c}^{(r',c)} P_{r',r}^{\neq c}$ for all i_c

e) discard $\boldsymbol{g}^{(r',c)}$

2) if $m < T$: discard $P_{r',r}^{\neq c}$

II) Rename $B_{r',r}^{\neq c} \leftarrow P_{r',r}^{\neq c}$

The memory cost of Algorithms 1-2 is $\mathcal{O}\left(R_\psi\left(R_\psi+n\right)\right)$, per vector computed in parallel (in addition to $\mathcal{O}\left(BR_\psi nD\right)$ required for storing the B vectors in the block). The factors of R_ψ^2 and nR_ψ come from storing the $B^{\neq c}$ matrix and right-hand-sides, respectively. The "ultra-low-memory" version saves a full $\mathcal{O}\left(TR_\psi^2\right)$ storage per vector compared to the low-memory version of I-RRBPM.

III. Results and Discussion

In this section we report vibrational energy levels of uracil and naphthalene, computed using the low-memory version of the Hierarchical Intertwined Reduced-Rank Block Power Method (HI-RRBPM).[32] These calculations could also be performed with the "ultra-low-memory" version, Algorithm 1, but we prefer to use the low-memory version because it requires less CPU time. As before, we parallelize the calculations over vectors in the blocks.

The potential energy surfaces we use are both "semi-diagonal" quartic Taylor expansions of the potential about the minimum energy geometry.[60] This simple form of the potential is convenient to use, although the method is compatible with any sum-of-products potential. The Hamiltonian is

$$\begin{aligned}\hat{H} &= \frac{\omega_c}{2}\left(\sum_{c=1}^{D}-\frac{\partial^2}{\partial q_c^2}+q_c^2\right) \\ &+ \frac{1}{6}\sum_{c_1=1}^{D}\sum_{c_2=1}^{D}\sum_{c_3=1}^{D}\phi^{(3)}_{c_1c_2c_3}q_{c_1}q_{c_2}q_{c_3} \\ &+ \frac{1}{24}\sum_{c_1=1}^{D}\sum_{c_2=1}^{D}\sum_{c_3=1}^{D}\sum_{c_4=1}^{D}\phi^{(4)}_{c_1c_2c_3c_4}q_{c_1}q_{c_2}q_{c_3}q_{c_4}\ , \end{aligned} \tag{9}$$

where we neglect all $\pi^t\mu\pi$ terms in the kinetic energy operator (KEO) and the potential-like $\sum_\alpha \mu_{\alpha,\alpha}$ term.[61] The number of terms in each node of a tree is reduced by sorting the terms in Eq. (1). See Ref. 35 for detail. The univariate functions, in Eq. (1) are eigenfunctions of 1D cut Hamiltonians obtained by keeping only the $\omega_c/2p_c^2$ term in the KEO and setting $q_{c'}=0, c'\neq c$ in the potential. They are obtained by solving each 1D cut Hamiltonian in a harmonic oscillator basis chosen large enough to converge the levels of interest.

A. Uracil ($C_4H_4O_2N_2$)

We have computed the lowest 224 vibrational states of the uracil molecule (Fig. 1), which has 12 atoms and 30 vibrational DOF. Uracil is essential to life as one of the four nucleobases of DNA; as such, its vibrational spectrum has been measured in numerous experiments spanning decades (see Ref. 62 for a complete list) and analysed in detail using second order vibrational perturbation theory.[62–66] The potential that we use is the quartic force field PES of Krasnoshchekov et al.,[62] which contains cubic and quartic anharmonic constants computed at the MP2/cc-pVTZ level. The harmonic frequencies of are the "best theoretical" harmonic constants computed earlier by Puzzarini et al.[64] With this PES, the Hamiltonian contains 30 kinetic, 30 harmonic potential, and 2716 cubic and 5050 quartic anharmonic potential terms, for a total of 7826 terms. The force constants are given in the Supplementary Material.

We find that some of the energy levels computed on this PES are spurious. Their energies change when we change the number of basis functions in some of the nodes. Some of them are lower than the level we identify as the zero point energy (ZPE). The quantum numbers assigned (using eigenvectors) to the spurious levels are usually nonsensical. Other levels are close to the VPT2 levels, as expected. The spurious levels exist because the PES has unphysical regions or holes. Along some cuts the potential increases and then decreases.

Such holes plague many polynomial PESs. Perturbation theory often works well even when the PES has holes. Hoping to find a PES without holes, we recomputed force constants at two different electronic structure levels: MO5-2X/6-311G, and MP2/cc-pVTZ level. Both the new PESs also have holes. They they are less severe for the MP2/cc-pVTZ potential, which has constants almost identical to those of Krasnoshchekov et al.[62] Since the MP2/cc-pVTZ PES of Krasnoshchekov et al[62] has fewer quartic terms (5050) than ours (11614), we used the potential from Ref. 62 for all the HI-RRBPM calculations.

We must do something to eliminate the holes without significantly changing the PES near the equilibrium geometry. The univariate cut potentials, $V_i(q_i)$ are large when $|q_i|$ is large; the holes are due to the coupling terms, $V_{coup} = V - \sum_i V_i(q_i)$. One way to deal with the problem is: 1) choose

a function $z(q_i)$ that approaches a plateau value as $|q_i|$ increases; 2) expand z_i in terms of q_i; 3) invert these expansions to obtain

$$q_i = \sum_k c_k z_i^k; \tag{10}$$

4) substitute $q_i = \sum_k c_k z_i^k$ into V_{coup} and retain only the lowest powers of z_i^k. This yields a new PES that is a sum of the original PES and a term, whose degree is larger than the degree of the original PES that makes the new PES more realistic at large $|q_i|$. Replacing q_i with $\sum_k c_k z_i^k$ in V_{coup} ensures that V_{coup} approaches a constant value as $|q_j| \to \infty$. The function we use is $z_j = \tanh(\xi \alpha_j q_j)$. Because the degree of the factors in the terms of V_{coup} is less than or equal to two, we can keep only the first term in Eq. (10), i.e., $q_j = \frac{z_j}{\xi \alpha_j}$. If $V_i(q_i)$ is even, α_j is defined as for a Rosen-Morse potential[67]

$$\alpha_j = \sqrt{\left| \frac{\phi_j^{(4)}}{8\phi_j^{(2)}} \right|}. \tag{11}$$

The larger $\phi_{jjjj}^{(4)}$ is, the more likely it is that an unphysical region occurs at a smaller value of q_j. When $\phi_{jjjj}^{(4)}$ is large, it is therefore best to choose α_j so that it is large and the plateau is reached at smaller values of q_j. If $V_i(q_i)$ is odd, α_j is defined

$$\alpha_j = \frac{\phi_j^{(3)}}{3\phi_j^{(2)}}. \tag{12}$$

This means that if the cubic constant is large the plateau is reached sooner, thus limiting unphysical behaviour. In the plateau region there is no coupling. In the $\tanh$ argument, ξ is an adjustable parameter. We need it because the above choices of α_j are somewhat arbitrary. As primitive basis functions, we use standard harmonic oscillator functions. To use the modified PES we must compute matrix elements of $\tanh(\xi \alpha_j q_j)$ in the harmonic basis. This is done by evaluating the required 1D integrals with a 257-point Clenshaw-Curtis quadrature in q_j.

Increasing ξ will remove holes because it moves the plateau region closer to the equilibrium geometry. Although all the non-zero derivatives (with respect to the q_α coordinates) of the original

PES are unchanged by replacing q_j with $\frac{z_j}{\xi \alpha_j}$, the shape of the potential close to the equilibrium geometry changes enough that energy levels are affected. If ξ is too small, holes remain. If ξ is too large, the modified coupling terms infringe on the region close to the equilibrium geometry. The hole problem exists only because the PESs we use are truncated Taylor series in normal coordinates If the PES were fit to a more physical form there would be no holes. For uracil, we found that with $\xi = 1.125$, the modified PES still has spurious levels. With $\xi = 1.25$, the modified PES has some, but fewer, spurious levels. With $\xi = 1.5$, there are no spurious levels and we assume no holes, however, all of the non-spurious levels are shifted up, compared to their $\xi = 1.25$ counterparts.

The tree used in the hierarchical calculations in this paper is shown in Figure 2. Since many of the low frequency modes $q_{18} - q_{30}$ couple strongly to the N-H stretch modes q_1 and q_2 and to the C-H stretch modes q_3 and q_4, it is necessary to retain many basis functions as one moves up the tree in order to obtain converged energy levels. For this reason, we arrange modes $q_1 - q_4$ and $q_{18} - q_{30}$ into small groups of 2-4 coordinates each and retain moderately large basis sizes, i.e. 166-236 functions throughout the tree. The intermediate frequency modes $q_5 - q_{17}$, which couple less strongly to $q_1 - q_4$ and $q_{18} - q_{30}$, are grouped together in several steps into a single node on the second-from-the-top layer. The number of states computed at the top node, 224, is enough to accurately compute the fundamentals below 1200 cm^{-1}, that is, $\nu_{13} - \nu_{30}$.

Parameters used in the calculations are summarized in Table 1. For $\xi = 1.25$, a preliminary calculation was performed with $R_\psi = 40$ (for all nodes) and $N_{cycle} = 20$. We then added 200-40=160 terms with random $\boldsymbol{f}^{(r,c)}$ whose normalization constants are small to the top-layer wavefunctions computed in this preliminary calculation to obtain initial guesses for a second top layer calculation with $R_\psi = 200$ and $N_{cycle} = 10$. The basis parameters, except R_ψ and N_{cycle}, for these calculations are the same as those in Table 1 for calculations 'A1'-'A4'. The top-layer wavefunctions from this second calculation, with $R_\psi = 200$, were then used as initial guesses (again small random terms were added so that the rank of the input vectors is equal to R_ψ) for the calculations labelled 'A1'-'A3' in Table 1. The 'B1'-'B3' calculations were done in the same way, but for $\xi = 1.50$. For $\xi = 1.25$, an additional calculation ('A4') was performed, re-computing again the top-layer wave-

functions using this time as initial vectors the top-layer wavefunctions from the 'A3' calculation (plus small random terms). Choosing $R_\psi = 40$ for nodes below the top is enough to converge the energy levels in these branch nodes; larger ranks are needed for top nodes only.

Table 2 lists selected levels of uracil for the 'A1'-'A4' and 'B1'-'B3' HI-RRBPM calculations. We report levels that we can unambiguously assign. To assign levels, we first use ALS to reduce the rank of the corresponding wavefunctions to one. If the assignments obtained by reducing the rank is unclear (e.g., if two wavefunctions are assigned the same labels) then we verify or correct them by computing eigenvectors. We also compare our fundamental transitions with the CVPT2 levels of Ref. 62. Since replacing q_j with $\frac{z_j}{\xi\alpha_j}$ changes the potential, the CVPT2 calculation and the 'A' and 'B' HI-RRBPM calculations are performed on different PESs. From Table 2 we observe that modifying the PES does not significantly affect low-lying fundamentals $\nu_{18} - \nu_{20}$, $\nu_{23} - \nu_{25}$, and $\nu_{28} - \nu_{30}$, whose HI-RRBPM values in both 'A' and 'B' sets converge to within $<$15 cm^{-1} of the CVPT2 values. Higher fundamentals are more strongly affected by the change in potential, and ν_{26} and ν_{27} are severely affected. However, the aim of this paper is not to produce a better PES for uracil but to demonstrate that it is possible to use a variational method to compute converged energy levels of a twelve-atom molecule.

Comparing the 'A3' and 'A4' levels enables one to assess the convergence of the 'A' calculations. Half of the reported levels change by < 1 cm^{-1} as the rank is increased from $R_\psi = 600$ to $R_\psi = 700$. Since the value $\xi = 1.25$ used in the 'A' set calculations does not fully remove the holes, the spectrum contains spurious energy levels some of whose energies are similar to those of levels that we want to compute. These spurious levels increase the density of the eigenvalue spectrum, which slows convergence of the power method. Without the holes, the true levels would converge faster. In the 'B' calculations, there is no indication that holes affect any of the levels of interest. Comparing 'B2' and 'B3', one sees that convergence is significantly better than in the 'A' set: all but eight of the reported levels decrease by < 1 cm^{-1} as the rank is increased from $R_\psi = 500$ to $R_\psi = 600$. The larger value of $\xi = 1.5$, used for the 'B' calculations, shifts the entire spectrum to higher energy. The 'B3' ZPE is larger than its 'A4' counterpart by ca. 24 cm^{-1}. Differences between 'B3' levels and the 'B3' ZPE are also larger than differences between 'A3' levels and the

'A3' ZPE. However, the tight convergence of the levels in 'B3' demonstrates that it is possible to compute converged energy levels for a 12-atom molecule, if the potential does not have holes in accessible regions.

B. Naphthalene (C_8H_{10})

In this subsection, we present HI-RRBPM calculations of the lowest 128 vibrational levels of naphthalene, with 18 atoms and 48 DOF. Amongst the 128 are the 20 lowest fundamentals. Naphthalene, the smallest polycyclic aromatic hydrocarbon (PAH), has been the subject of several recent theoretical[68–73] and experimental[72–77] spectroscopic studies due to the importance of PAHs as pollutants[78] and as possible carriers of the Aromatic Infrared Bands[79] observed in space. The spectrum of naphthalene has been computed with second order vibrational perturbation theory by several authors.[68,69,71–73] The PES we use is a quartic force field computed at the B9-71/TZ2P density functional level and is available in the Supplementary Material of Ref. 69. Quartic force fields for naphthalene have also been computed by other authors using the same or different electronic structure methods.[68,71–73] The PES that we use contains 48 harmonic constants and 1936 and 2189 cubic and quartic anharmonic constants, respectively. Including kinetic terms, the Hamiltonian has 4221 terms and has the form of Eq 9. We did not encounter problems with holes for this PES, and therefore it is used without modification.

The tree used in the naphthalene HI-RRBPM calculations is shown in Figure 4. Following the strategy used previously, we arrange the coordinates into groups with similar frequencies and types of motion in lower layers of the tree. As in our previous papers, we find that it is not necessary to optimize the placement of coordinates in the tree to compute accurate energy levels. We arrange the nodes in a quasi-binary fashion in all layers below the top; this has the advantage that most of the nodes have $d = 2$ sub-nodes, in which case one can use singular value decomposition (SVD) to reduce the ranks. In the third layer from the bottom, we use standard diagonalization to compute the bases for nodes containing two sub-nodes, instead of the power method, since the direct product basis is small. The direct product sizes shown for these nodes are larger than is

necessary for computing accurate bases in higher levels of the tree. Therefore we truncate the bases to smaller sizes in the fourth layer. The top node, in which we combine the six nodes from the previous layer, is the only node where we use the I-RRBPM and accounts for the vast majority of the calculation time.

We made seven HI-RRBPM calculations with R_ψ values between 60 and 1000. Parameters for the calculations are given in Table 3. The bases for all nodes below the top were all computed with $R_\psi = 60$. Calculations 'B'-'G' differ from calculation 'A' only because the functions of the top node are re-computed with a larger rank, using input vectors obtained from the top layer of a previous calculation (and small random terms). For calculation 'B' the input vector is made from the top layer of calculation 'A'. For calculation 'C' the input vector is made from the top layer of calculation 'B'. For calculation 'D' the input vector is made from the top layer of calculation 'C'. For calculation 'E' the input vector is made from the top layer of calculation 'C'. For calculation 'F' the input vector is made from the top layer of calculation 'E'. For calculation 'G' the input vector is made from the top layer of calculation 'F'. Calculations 'D' and 'E' are done in parallel. This strategy was also used previously in calculations on cyclopentadiene.[32] It makes it possible to do inexpensive calculations for the nodes in lower layers of the tree where small ranks are sufficient and at the top of the tree, where a large rank is needed, a large rank calculation. The number of cycles for calculations 'B', 'C', 'D','E', 'F', 'G' is fairly small (see table 3), only large enough to converge the levels for the corresponding rank.

Table 4 lists the lowest 128 energy levels of naphthalene from the HI-RRBPM calculations. Experimental values for the fundamentals and VPT2 values from Ref. 69 are also shown, where available. The energy levels decrease significantly as the rank is increased from $R_\psi = 60$ to $R_\psi = 300$ and more slowly as the rank is increased from $R_\psi = 300$ to $R_\psi = 1000$. Comparing the 'F' and 'G' columns provides a rough estimate of convergence. Most of the levels in the bottom half of the spectrum are well-converged and decrease by less than 1 cm^{-1} when the rank is increased from $R_\psi = 700$ to $R_\psi = 1000$. Moreover, most of the HI-RRBPM fundamentals are close to (and in some cases, lower than) the VPT2 values in the largest 'G' calculation. Levels in the top half of the spectrum are less converged, with the largest absolute change between the 'F' and 'G'

being 11.5 cm^{-1} for the $3\nu_{13} + 2\nu_{48}$ level. Increasing either the block size B, the rank R_ψ, or the number of cycles N_{cyc} would improve these levels. Differences between the variational and the VPT2 energies are small.

Calculations on naphthalene are time consuming but require relatively little memory. For example, the 'F' calculation has a total memory cost of 364 GB, of which 358 GB are used to store P matrices. If the ultra-low-memory version were used and the calculation run on 128 processors, 'F' would require only 4.7 GB. This includes 0.5 GB for Hamiltonian operator matrices and 3.0 GB for storing two copies of the vectors in the block during the vector update step, both of which do not depend on the number of processors. Using the ultra-low-memory version, the CPU cost would be approximately twice as high, owing to the fact that the top-layer node contains six sub-nodes.

We use many processors (see Tables 1 and 3). If, instead, it were possible to use only 8, calculation 'F', with the ultra-low-memory version, would need 3.6 GB in total although the CPU cost would be much higher. However, this memory cost is small enough that it would be possible to fit the Hamiltonian and the basis vectors onto a graphical processing unit (GPU) card. MVPs and vector inner products account for the majority of the computational burden; these operations can be subdivided into small parallelizable chunks. Thus, the ultra-low-memory HI-RRBPM could be used to perform variational quantum dynamics calculations on molecules with over a dozen atoms using a fairly common workstation.

IV. Conclusion

Variational methods have been used to compute vibrational spectra for decades. The first calculations were done with orthonormal basis functions by explicitly constructing and diagonalizing a Hamiltonian matrix. The computation time required to diagonalize a matrix scales as N^3, where N is the size of the matrix. Fortunately, the speed of computers has improved significantly. However, to diagonalize a matrix with standard algorithms, it must be stored in memory. If the computer one is using does not have enough memory to store the matrix, it is not possible to compute a spectrum by diagonalization. Important progress was made by using iterative eigensolvers to compute

some, but not all of the eigenvalues of a Hamiltonian matrix. To use an iterative eigensolver there is no need to store a Hamiltonian matrix in memory. It is, however, necessary to store in memory vectors with has many elements as there are basis functions. For molecules with more than about five atoms this means that it is not possible, even with iterative eigensolvers, to compute spectra with a direct product basis. One way to beat this problem is to use a nondirect product basis.

It is also possible to use a variational method with a direct product basis and to solve the vibrational Schroedinger equation *without storing vectors with has many elements as there are direct product basis functions*. This is done by reducing the rank of basis vectors.[31,32,35,50,53] The memory required scales linearly (not exponentially) with the number of degrees of freedom. In this paper, we report calculations, done with reduced-rank basis vectors, on uracil and naphthalene with 12 and 18 atoms. This is done by using a sequence of basis contractions organized into a tree[35] and the intertwining idea to decrease the cost of the rank reduction.[32] The method was dubbed the HI-RRBPM. We also suggest a new ultralow memory version of the HI-RRBPM, which further reduces the required memory. With the ultralow memory version, variational calculations on molecules with more than a dozen atoms are possible on a common desktop computer. It might be possible to use similar ideas to solve the time-dependent Schroedinger equation.

V. Acknowledgment

This work was supported by the Natural Sciences and Engineering Research Council of Canada. Calculations were done on computers purchased with money from the Canada Foundation for Innovation. JA and HFS were supported by the U.S. National Science Foundation, Grant CHE-1661604

References

[1] J. Bloino and V. Barone, J. Chem. Phys. 136 124108 (2012)

[2] J. Tennyson, Comp. Phys. Rep. **4**, 1 (1986).

[3] S. Carter and N. C. Handy, Comput. Phys. Com. **51**, 49 (1988).

[4] Tucker Carrington, *J. Chem. Phys.* **146**, 120902 (2017)

[5] M. J. Bramley and T. Carrington, The Journal of chemical physics 99, 8519-8541 (1993)

[6] J. Bowman, T. Carrington and H.-D. Meyer, Mol. Phys. 106, 2145-2182 (2008)

[7] AG Csaszar, C Fabri, T Szidarovszky, E Matyus, T Furtenbacher, G Czako Physical Chemistry Chemical Physics 14 (3), 1085-1106 (2012)

[8] R. Chen, G. Ma and H. Guo, The Journal of Chemical Physics 114 4763-4774 (2001)

[9] Christophe Iung and Claude Leforestier J. Chem. Phys. 102, 8453 (1995)

[10] Bastiaan J. Braams and Joel M. Bowman , International Reviews in Physical Chemistry, 28, 577, (2009).

[11] Moumita Majumder and Steve Alexandre Ndengue and Richard Dawes, Molecular Physics, 114, 1, (2016).

[12] Claude Leforestier, Linda B. Braly, Kun Liu, Matthew J. Elrod, and Richard J. Saykally J. Chem. Phys. 106, 8527 (1997).

[13] D. Gottlieb and S. Orszag, Numerical Analysis of Spectral Methods (Society for Industrial and Applied Mathematics, 1977).

[14] J. C. Light and T. Carrington Jr. Advances in Chemical Physics 114 263-310 (2000)

[15] G. Avila and T. Carrington Jr. The Journal of chemical physics 131.17 (2009): 174103.

[16] Gustavo Avila and Tucker Carrington Jr. J. Chem. Phys. 134, 054126 (2011)

[17] Sergei Manzhos and Tucker Carrington Jr J. Chem. Phys.145, 224110-1– 224110-9 (2016)

[18] X-G Wang and T. Carrington Jr J. Chem. Phys. 138, 104106-1 – 104106-20 (2013)

[19] Gustavo Avila and Tucker Carrington, J. Chem. Phys. 143, 214108 (2015)

[20] Grady D. Carney, Ludwig L. Sprandel, and C. William Kern, Adv. Chem. Phys., 37, 305 (1978)

[21] B. Poirier, J. Theor. Comput. Chem. 02, 65 (2003).

[22] R. Dawes and T. Carrington, J. Chem. Phys. 122, 134101 (2005).

[23] L. Halonen, D. W. Noid, and M. Child, J. Chem. Phys. 78, 2803 (1983).

[24] S. Carter, S. J. Culik, and J. M. Bowman, J. Chem. Phys. 107, 10458 (1997).

[25] R. Garnier, M. Odunlami, V. Le Bris, D. Begue, I. Baraille, and O. Coulaud, J. Chem. Phys. 144, 204123 (2016).

[26] H. R. Larsson, B. Hartke, and D. J. Tannor, J. Chem. Phys. 145, 204108 (2016)

[27] Marat Sibaev and Deborah L. Crittenden, The Journal of Chemical Physics 145, 064106 (2016);

[28] J. Cooper and T. Carrington Jr J. Chem. Phys. 130, 214110 (2009)

[29] James Brown and Tucker Carrington Jr., J. Chem. Phys.145, 144104 (2016)

[30] R. Barrett and M. Berry and T. F. Chan and J. Demmel and J. Donato and J. Dongarra and V. Eijkhout and R. Pozo and C. Romine and H. Van der Vorst , Templates for the Solution of Linear Systems: Building Blocks for Iterative Methods, 2nd Edition, SIAM, 1994, Philadelphia, PA

[31] A. Leclerc and T. Carrington, *J. Chem. Phys.* **140**, 174111 (2014).

[32] P. S. Thomas and T. Carrington Jr., *J. Chem. Phys.* **146**, 204110 (2017).

[33] G. Beylkin and M. J. Mohlenkamp, SIAM J. Sci. Comput. 26, 2133 (2005).

[34] T. G. Kolda and B. W. Bader, *SIAM Review* **51**, 455 (2009).

[35] P. S. Thomas and T. Carrington Jr., *J. Phys. Chem. A* **119**, 13074 (2015).

[36] A. Leclerc and T. Carrington Jr., *Chem. Phys. Lett.* **644**, 183 (2016).

[37] A. Leclerc, P. S. Thomas, and T. Carrington Jr., *Mol. Phys.* , DOI: 10.1080/00268976.2016.1249980 (2016).

[38] U. Manthe, H.-D. Meyer, and L. S. Cederbaum, J. Chem. Phys. 97, 3199 (1992).

[39] M. H. Beck, A. Jaeckle, G. A. Worth, and H.-D. Meyer, Phys. Rep. 324, 1 (2000).

[40] Ledyard R. Tucker, Psychometrika. 31, 279 (1966)

[41] H. Wang and M. Thoss, J. Chem. Phys. 119, 1289 (2003).

[42] U. Manthe, J. Chem. Phys. 128, 164116 (2008

[43] O. Vendrell and H.-D. Meyer, J. Chem. Phys. 134, 044135 (2011).

[44] R. Wodraszka and T. Carrington, Jr., J. Chem. Phys. 145, 044110 (2016).

[45] H. R. Larsson, B. Hartke, and D. J. Tannor, J. Chem. Phys. 145, 204108 (2016).

[46] R. Wodraszka and T. Carrington, Jr., J. Chem. Phys. 146, 194105 (2017).

[47] H. R. Larsson and D. J. Tannor, J. Chem. Phys. 147, 044103 (2017).

[48] P. Seidler, M. B. Hansen, and O. Christiansen, J. Chem. Phys. 128, 154113 (2008).

[49] Niels Kristian Madsen, Ian H. Godtliebsen, Sergio A. Losilla„ and Ove Christiansen The Journal of Chemical Physics 148, 024103 (2018)

[50] M. Rakhuba and I. Oseledets, J. Chem. Phys. 145, 124101 (2016).

[51] K. H. Marti and M. Reiher, Z. Phys. Chem. 224,. 583?599 (2010).

[52] Roberto Olivares-Amaya, Weifeng Hu,Naoki Nakatani, Sandeep Sharma, Jun Yang, and Garnet Kin-Lic Chan, THE JOURNAL OF CHEMICAL PHYSICS 142, 034102 (2015)

[53] Jonathan Jerke, and Bill Poirier J. Chem. Phys. 148, 104101 (2018);

[54] M. Rakhuba and I. Oseledets, *J. Chem. Phys.* **145**, 124101 (2016).

[55] S. Carter and N. C. Handy, Comput. Phys. Commun. 51, 49 (1988)

[56] X.-G. Wang and T. Carrington J. Chem. Phys. 117, 6923 (2002)

[57] P. Cassam-Chenai, J. Liévin, J. Comput. Chem. 27, 627 (2006)

[58] G. Beylkin and M. J. Mohlenkamp, *SIAM J. Sci. Comput.* **26**, 2133 (2005).

[59] G. H. Golub and C. F. V. Loan, *Matrix Computations, 3rd ed,*, John Hopkins University Press, Baltimore, MD, 1996.

[60] I. M. Mills, *Vibration-Rotation Structure in Asymmetric and Symmetric Top Molecules*, volume 1, p. 115, Academic Press, New York, 1972.

[61] J. K. G. Watson, *Molec. Phys.* **15**, 479 (1968).

[62] S. V. Krasnoshchekov, N. Vogt, and N. F. Stepanov, *J. Phys. Chem. A* **119**, 6723 (2015).

[63] G. N. Ten, V. V. Nechaev, and S. V. Krasnoshchekov, *Optics and Spectrosc.* **108**, 37 (2010).

[64] C. Puzzarini, M. Biczysko, and V. Barone, *J. Chem. Theor. Comput.* **7**, 3702 (2011).

[65] T. Fornaro, M. Biczysko, S. Monti, and V. Barone, *Phys. Chem. Chem. Phys.* **16**, 10112 (2014).

[66] T. Fornaro, I. Carnimeo, and M. Biczysko, *J. Phys. Chem. A* **119**, 5313 (2015).

[67] Tucker Carrington Molecular Physics, 70, 757-766, (1990)

[68] V. Librando, A. Alparone, and Z. Minniti, *J. Mol. Struct. (THEOCHEM)* **847**, 23 (2007).

[69] E. Cané, A. Miani, and A. Trombetti, *J. Phys. Chem. A* **111**, 8218 (2007).

[70] M. Basire, P. Parneix, F. Calvo, T. Pino, and P. Bréchignac, *J. Phys. Chem. A* **113**, 6947 (2009).

[71] J. Bloino, *J. Phys. Chem. A* **119**, 5269 (2015).

[72] C. J. Mackie, A. Candian, X. Huang, E. Maltseva, A. Petrignani, J. Oomens, W. J. Buma, T. J. Lee, and A. G. G. M. Tielens, *J. Chem. Phys.* **143**, 224314 (2015).

[73] S. Chakraborty, S. Banik, and P. K. Das, *J. Phys. Chem. A* **120**, 9707 (2016).

[74] O. Pirali, M. Goubet, T. R. Huet, R. Georges, P. Soulard, P. Asselin, J. Courbe, P. Roy, and M. Vervloet, *Phys. Chem. Chem. Phys.* **15**, 10141 (2013).

[75] O. Pirali, N.-T. Van-Oanh, P. Parneix, M. Vervloet, and P. Bréchignac, *Phys. Chem. Chem. Phys.* **8**, 3707 (2006).

[76] O. Pirali, M. Vervloet, G. Mulas, G. Malloci, and C. Joblin, *Phys. Chem. Chem. Phys.* **11**, 3443 (2009).

[77] S. Albert, K. K. Albert, P. Lerch, and M. Quack, *Faraday Discuss.* **150**, 71 (2011).

[78] K. Ravindra, R. Sokhi, and R. van Grieken, *Atmos. Environ.* **42**, 2895 (2008).

[79] A. Léger and J. Puget, *Astron. Astrophys.* **137**, L5 (1984).

Table 1: Parameters for HI-RRBPM calculations on uracil. Wall times in this paper were obtained using Intel E7-8867 (v3) processors running at 2.5 GHz. R_ψ is for the calculation of the top node only.

Parameter	Value						
Calculation:	A1	A2	A3	A4[a]	B1	B2	B3
ξ	1.25	1.25	1.25	1.25	1.50	1.50	1.50
R_ψ	400	500	600	700	400	500	600
N_{CPU}	32	56	112	75	56	56	112
$N^b_{ALS;\psi}$	2	2	2	2	2	2	2
N_{cyc}	10	10	10	10	10	10	10
N_{sweep}	10	10	10	10	10	10	10
Memory (GB)	26	65	181	166	43	65	181
Wall time (d)	18.8	14.6	15.8	35.0	8.9	14.5	13.3

[a] Continuation of 'A3' calculation with larger rank

[b] For rank reductions in Gram-Schmidt, $\mathbf{H}^{(\mathcal{F})} = \mathcal{F}^T\mathbf{H}\mathcal{F}$ steps; $N_{ALS;\psi} = 10$ in vector updates

Table 2: Lowest vibrational energy levels (cm^{-1}) computed for uracil using HI-RRBPM, in comparison to CVPT2 values from Ref. 62. We report the zero-point energy (ZPE) and differences between other levels and the ZPE.

CVPT2	HI-RRBPM							
	A1	A2	A3	A4	B1	B2	B3	Assignment
	18969.36	18969.27	18969.21	18969.12	18993.14	18993.07	18993.02	ZPE
139.7	140.22	140.15	140.10	140.02	143.90	143.87	143.84	ν_{30}
157.9	157.29	157.21	157.16	157.09	159.20	159.17	159.15	ν_{29}
	295.60	295.15	294.95	294.53	296.53	296.47	296.41	$2\nu_{30}$
	311.51	311.00	310.68	310.02	303.56	303.48	303.42	$\nu_{30}+\nu_{29}$
	327.21	326.73	326.38	325.66	324.39	324.30	324.24	$2\nu_{29}$
	385.50	385.37	385.30	385.15	385.18	385.14	385.12	ν_{21}
384.4	379.97	379.76	379.68	379.36	386.37	386.31	386.27	ν_{28}
510.8	511.10	511.01	510.91	510.81	511.49	511.45	511.43	ν_{20}
	514.57	513.84	513.40	512.49	528.56	528.32	528.14	$\nu_{30}+\nu_{28}$
	526.14	525.91	525.75	525.43	529.83	529.62	529.49	$\nu_{30}+\nu_{21}$
531.1	535.67	535.23	535.13	535.08	533.04	532.83	532.68	ν_{19}
535.3	546.04	545.52	545.08	543.15	536.79	536.67	536.56	ν_{18}
	543.43	543.10	543.00	542.77	545.08	544.95	544.87	$\nu_{29}+\nu_{21}$
	530.69	530.07	529.64	528.68	551.42	551.24	551.10	$\nu_{29}+\nu_{28}$
	653.35	652.23	651.73	651.91	655.56	655.45	655.37	$\nu_{30}+\nu_{20}$
	669.84	668.42	669.34	669.86	671.35	671.24	671.13	$\nu_{29}+\nu_{20}$
	672.22	678.57	679.03	676.87	679.00	678.58	678.37	$\nu_{30}+\nu_{19}$
	690.39	689.18	688.56	687.46	692.23	691.67	691.38	$\nu_{29}+\nu_{19}$
715.8	704.62	702.24	711.51	705.29	713.39	713.16	712.94	ν_{25}
549.4	725.78	724.71	726.81	725.85	740.53	740.43	740.39	ν_{27}
756.1	754.70	754.14	754.90	754.47	754.84	754.77	754.74	ν_{24}
751.8	779.37	780.92	780.88	778.02	764.88	764.75	764.65	ν_{17}
	772.12	772.12	771.98	770.91	770.96	770.88	770.82	$2\nu_{21}$
	765.47	766.99	766.99	766.39	771.92	771.71	771.61	$\nu_{21}+\nu_{28}$
	761.27	760.93	762.38	759.56	789.30	789.07	788.88	$2\nu_{28}$
651.4	789.95	791.44	791.50	789.99	805.57	805.39	805.27	ν_{26}
803.2	819.10	809.16	804.65	798.73	808.83	809.18	808.92	ν_{23}
	865.24	864.20	865.47	867.69	883.02	882.45	882.02	$\nu_{30}+\nu_{27}$
	901.59	901.95	902.13	900.75	898.54	897.83	897.46	$\nu_{21}+\nu_{20}$
	894.19	896.64	896.26	894.00	899.65	898.53	898.03	$\nu_{28}+\nu_{20}$
	902.62	898.70	898.32	899.38	902.47	901.04	900.66	$\nu_{30}+\nu_{24}$
	888.36	886.27	886.72	886.53	903.82	901.62	901.46	$\nu_{29}+\nu_{27}$
	923.57	925.82	922.96	917.80	910.26	909.40	908.86	$\nu_{30}+\nu_{17}$
	918.47	920.89	919.88	916.42	918.60	916.37	915.91	$\nu_{29}+\nu_{24}$

Table 2: (continued)

CVPT2	HI-RRBPM							
	A1	A2	A3	A4	B1	B2	B3	Assignment
	928.36		924.56	924.45	921.93	919.71	919.29	$\nu_{21} + \nu_{19}$
		929.57	926.27	934.89	925.86	924.79	923.61	$\nu_{21} + \nu_{18}$
	930.96		928.26	928.78	929.64	927.56	927.15	$\nu_{20} + \nu_{17}$
	941.29	939.79	935.68	933.56	950.77	949.54	949.15	$\nu_{30} + \nu_{26}$
	951.42		951.46	946.24	952.43	951.72	950.77	$\nu_{30} + \nu_{23}$
947.5	969.98	967.69	965.55	966.07	962.00	960.94	960.34	ν_{16}
	954.60	951.95	948.09	948.41	965.80	965.03	964.69	$\nu_{29} + \nu_{26}$
955.9	974.87	969.96	970.39	961.82	975.61	972.40	971.14	ν_{22}
979.9	1001.02	998.68	998.30	998.23	997.61	996.30	995.56	ν_{15}
	1034.49	1026.54	1032.44	1027.19	1030.83	1027.40	1026.27	$2\nu_{20}$
	1051.36	1047.28	1047.51	1050.40	1050.63	1048.80	1048.94	$\nu_{30} + \nu_{19}$
	1126.87	1121.96	1120.91	1115.95	1136.77	1134.35	1128.43	$\nu_{27} + \nu_{21}$
	1152.13	1144.88	1144.81	1143.28	1149.46	1146.22	1144.15	$\nu_{21} + \nu_{14}$
	1150.98	1141.44	1140.75	1136.93	1149.34	1146.84	1146.03	$\nu_{28} + \nu_{14}$
	1157.39	1156.72	1150.06	1145.01	1163.85	1159.03	1156.53	$\nu_{28} + \nu_{17}$
	1188.87	1183.52	1178.93	1179.67	1205.22	1198.78	1196.00	$\nu_{26} + \nu_{21}$
1179.9	1209.64	1208.59	1205.45	1203.81	1208.62	1207.24	1205.80	ν_{13}

Table 3: Parameters for HI-RRBPM calculations on naphthalene. Wall times in this paper were obtained using Intel E7-8867 (v3) processors running at 2.5 GHz. R_ψ is for calculation of the top node only.

Parameter	A	B[a]	C[b]	D[c]	E[c]	F[d]	G[e]
R_ψ	60	300	400	500	600	700	1000
N_{CPU}	128	128	128	64	64	128	64
$N^f_{ALS_\psi}$	2	2	2	2	2	2	2
N_{cyc}	20	10	10	20	10	10	5
N_{sweep}	10	10	10	10	10	10	10
Memory (GB)	10	68	120	94	135	364	371
Wall time (d)	0.38	2.1	4.9	25.4	21.0	18.8	41.4

[a]Continuation of 'A' calculation with larger rank
[b]Continuation of 'B' calculation with larger rank
[c]Continuation of 'C' calculation with larger rank
[d]Continuation of 'E' calculation with larger rank
[e]Continuation of 'F' calculation with larger rank
[f]For rank reductions in Gram-Schmidt, $\mathbf{H}^{(\boldsymbol{\mathcal{F}})} = \boldsymbol{\mathcal{F}}^T \mathbf{H} \boldsymbol{\mathcal{F}}$ steps; $N_{ALS_\psi} = 10$ in vector updates

Table 4: Lowest 128 vibrational levels (cm^{-1}) computed for naphthalene using HI-RRBPM. Experimental and VPT2 fundamental values are taken from Table I of Ref.[69] except where noted.

Exp	VPT2	HI-RRBPM							Assignment
		A	B	C	D	E	F	G	
		31782.20	31768.71	31767.75	31767.13	31766.87	31766.50	31766.03	ZPE
166.6584388[a]	166	165.84	165.80	165.36	165.06	164.92	164.79	164.60	ν_{48}
	177	184.90	179.21	178.86	178.62	178.51	178.36	178.18	ν_{13}
		338.21	332.11	330.96	330.36	330.17	329.82	329.41	$2\nu_{48}$
		365.68	345.16	343.78	343.05	342.76	342.47	342.02	$\nu_{13}+\nu_{48}$
358.7[b]	359	372.86	357.92	355.80	355.21	355.05	354.85	354.44	ν_{24}
		397.32	361.10	359.70	358.94	358.52	358.20	357.66	$2\nu_{13}$
390	383	405.35	388.88	388.24	388.04	387.95	387.84	387.71	ν_{16}
465	466	468.20	464.87	464.23	463.97	463.87	463.71	463.47	ν_{28}
473.739502[a]	473	477.10	473.78	473.17	472.93	472.83	472.63	472.41	ν_{47}
		506.60	500.30	498.16	497.10	496.71	496.14	495.50	$3\nu_{48}$
509	508	513.63	509.00	506.88	506.14	505.81	505.87	505.64	ν_{44}
		534.62	514.89	512.79	510.73	510.18	509.61	508.43	$\nu_{13}+2\nu_{48}$
513	512	552.53	517.51	514.53	513.71	513.31	512.95	512.32	ν_9
		573.62	525.47	524.97	523.03	521.72	521.14	520.31	$\nu_{24}+\nu_{48}$
		577.47	530.42	527.56	525.37	524.60	523.66	522.83	$2\nu_{13}+\nu_{48}$
		581.62	537.65	534.19	533.48	533.14	532.62	531.90	$\nu_{24}+\nu_{13}$
		583.38	543.28	540.96	538.87	538.49	537.96	537.32	$3\nu_{13}$
		602.68	556.57	554.92	554.33	554.15	553.87	553.44	$\nu_{16}+\nu_{48}$
		610.60	569.04	568.08	567.53	567.37	567.11	566.73	$\nu_{16}+\nu_{13}$
619.5[b]	624	626.99	624.26	623.30	622.14	621.93	621.76	621.30	ν_{36}
	621	646.39	626.63	625.28	624.57	624.47	624.37	624.12	ν_{12}
		652.64	632.91	630.82	630.08	629.85	629.45	628.94	$\nu_{28}+\nu_{48}$
		664.85	644.08	642.53	641.65	641.47	641.09	640.45	$\nu_{47}+\nu_{48}$
		674.81	645.74	644.85	644.21	643.95	643.60	643.04	$\nu_{28}+\nu_{13}$
		692.32	655.36	654.63	653.97	653.78	653.49	652.85	$\nu_{47}+\nu_{13}$
		695.81	671.98	668.42	667.19	666.60	665.84	664.98	$4\nu_{48}$
		710.41	680.31	675.83	673.98	673.29	672.42	671.45	$\nu_{44}+\nu_{48}$
		716.49	684.60	683.23	680.17	678.31	677.70	676.34	$\nu_{13}+3\nu_{48}$
		732.70	689.47	685.16	683.94	682.21	680.53	680.36	$\nu_9+\nu_{48}$
		735.97	698.72	692.46	690.08	689.55	687.94	686.06	$\nu_{44}+\nu_{13}$
		751.01	702.06	696.11	693.33	692.19	690.70	688.11	$\nu_{24}+2\nu_{48}$
		754.62	705.91	699.96	697.89	695.39	694.02	691.73	$2\nu_{13}+2\nu_{48}$
		763.88	713.19	702.40	699.17	697.17	696.47	693.84	$\nu_9+\nu_{13}$
		779.99	716.95	708.15	703.13	701.65	700.09	698.49	$\nu_{24}+\nu_{13}+\nu_{48}$

Table 4: (continued)

Exp	VPT2	HI-RRBPM							Assignment
		A	B	C	D	E	F	G	
		784.81	718.12	712.39	710.56	708.45	706.25	705.54	$3\nu_{13}+\nu_{48}$
726	714	798.16	723.68	717.23	714.65	711.19	710.68	708.09	ν_{15}
		802.45	731.20	720.66	716.82	717.16	715.46	712.48	$2\nu_{24}$
		805.08	735.23	727.19	718.82	718.31	716.75	713.69	$\nu_{24}+2\nu_{13}$
		808.73	739.88	729.95	726.20	725.63	723.44	721.82	$4\nu_{13}$
		823.73	741.87	733.81	729.46	726.54	726.18	724.15	$\nu_{16}+2\nu_{48}$
		825.38	750.18	738.83	735.03	734.50	733.87	732.90	$\nu_{16}+\nu_{13}+\nu_{48}$
		832.18	754.85	752.18	745.91	744.18	743.26	742.22	$\nu_{24}+\nu_{16}$
		835.56	756.48	753.86	749.83	749.32	748.56	747.58	$\nu_{16}+2\nu_{13}$
764	757	838.23	767.84	764.02	759.51	758.52	757.39	756.63	ν_8
773	768	842.07	775.48	772.93	772.03	772.04	771.83	771.57	ν_{27}
782.330968[a]	783	844.94	778.73	777.70	774.98	774.71	774.08	773.40	ν_{46}
		852.27	786.31	783.25	781.52	781.07	780.71	779.96	$2\nu_{16}$
		854.02	795.55	793.21	793.16	791.25	788.97	787.48	$\nu_{36}+\nu_{48}$
		855.73	798.30	795.91	795.25	794.40	792.81	791.83	$\nu_{12}+\nu_{48}$
796	794	857.32	808.51	799.67	795.46	795.67	793.66	793.54	ν_{23}
		860.55	810.90	804.84	801.91	800.63	799.73	798.51	$\nu_{28}+2\nu_{48}$
		865.57	812.54	808.33	805.08	804.53	803.25	802.17	$\nu_{30}+\nu_{13}$
		869.67	816.38	810.60	808.07	807.88	806.78	805.87	$\nu_{12}+\nu_{13}$
		881.02	819.05	817.01	815.87	813.30	813.88	812.49	$\nu_{47}+2\nu_{48}$
		883.37	822.25	818.46	817.08	815.74	814.40	812.63	$\nu_{28}+\nu_{13}+\nu_{48}$
		891.19	833.47	831.36	826.96	824.32	823.63	821.00	$\nu_{24}+\nu_{28}$
		892.59	834.40	834.05	829.98	827.72	826.48	824.15	$\nu_{47}+\nu_{13}+\nu_{48}$
		895.59	836.77	836.32	831.80	829.04	829.78	827.44	$\nu_{28}+2\nu_{13}$
		905.47	842.85	837.66	833.57	833.04	832.12	829.58	$\nu_{24}+\nu_{47}$
	830	910.82	846.61	848.08	840.98	834.79	832.66	830.65	ν_{11}
		914.53	850.84	850.42	843.63	840.61	839.33	838.23	$\nu_{47}+2\nu_{13}$
		915.26	859.91	857.49	850.29	846.24	846.72	841.94	$\nu_{44}+2\nu_{48}$
		919.13	865.41	861.97	857.40	853.59	851.53	848.19	$\nu_9+2\nu_{48}$
		929.98	867.77	863.25	858.21	856.43	854.56	850.51	$5\nu_{48}$
		932.38	874.67	865.99	863.48	860.61	857.81	854.09	$\nu_{44}+\nu_{13}+\nu_{48}$
		940.69	879.09	872.04	865.49	861.97	860.26	858.45	$\nu_{13}+4\nu_{48}$
		942.34	884.46	873.27	868.58	865.45	864.87	858.93	$\nu_{24}+3\nu_{48}$
		945.46	886.80	874.21	871.95	868.27	866.84	860.27	$\nu_{16}+\nu_{28}$
		951.31	888.56	877.63	873.60	870.46	868.47	865.36	$\nu_9+\nu_{13}+\nu_{48}$
		957.75	890.32	880.76	875.92	872.57	872.98	866.89	$\nu_{24}+\nu_{44}$
		964.89	895.25	884.26	878.91	875.10	875.72	870.84	$2\nu_{13}+3\nu_{48}$

Table 4: (continued)

Exp	VPT2	HI-RRBPM							Assignment
		A	B	C	D	E	F	G	
		966.28	899.25	884.80	880.05	877.17	876.86	871.53	$\nu_9 + \nu_{24}$
		973.24	900.77	890.72	881.36	879.37	877.38	871.97	$\nu_{16} + \nu_{47}$
		974.53	905.03	895.27	885.68	882.73	878.85	873.66	$\nu_{24} + \nu_{13} + 2\nu_{48}$
		977.60	908.53	899.28	887.39	885.16	881.00	875.87	$\nu_{44} + 2\nu_{13}$
		981.99	911.26	901.77	888.60	888.99	882.96	878.03	$\nu_9 + 2\nu_{13}$
		987.98	916.32	903.11	890.26	891.37	886.61	880.02	$\nu_{15} + \nu_{48}$
		989.84	917.98	907.54	891.64	895.67	889.11	880.57	$2\nu_{24} + \nu_{48}$
		992.82	921.39	911.58	899.65	899.00	891.07	885.24	$\nu_{24} + 2\nu_{13} + \nu_{48}$
880	877	993.75	924.37	913.73	905.28	900.93	894.93	887.53	ν_{26}
		999.73	926.45	916.74	907.79	902.75	897.15	889.43	$\nu_{15} + \nu_{13}$
		1003.95	927.17	918.44	909.34	904.57	901.57	890.57	$3\nu_{13} + 2\nu_{48}$
		1006.17	929.14	920.54	911.05	905.71	903.77	895.62	$2\nu_{24} + \nu_{13}$
		1010.40	930.99	922.01	913.68	907.53	905.86	897.87	$4\nu_{13} + \nu_{48}$
		1012.03	933.37	925.43	916.26	909.09	907.98	899.47	$\nu_{24} + 3\nu_{13}$
		1014.53	934.75	928.79	919.10	912.50	909.03	901.79	$\nu_{16} + 3\nu_{48}$
		1019.32	940.36	930.81	919.73	914.39	910.15	906.00	$\nu_{44} + \nu_{16}$
		1021.74	943.50	932.38	923.84	915.84	912.71	907.65	$\nu_9 + \nu_{16}$
		1024.48	943.81	932.97	924.45	919.35	913.97	911.06	$\nu_{16} + \nu_{13} + 2\nu_{48}$
		1026.59	945.77	936.38	927.59	922.42	917.99	913.81	$5\nu_{13}$
		1029.54	948.09	938.94	929.03	924.58	919.74	914.94	$\nu_{24} + \nu_{16} + \nu_{48}$
		1032.04	950.20	941.04	933.77	926.50	923.31	920.33	$\nu_{16} + 2\nu_{13} + \nu_{48}$
		1036.19	952.36	941.73	934.11	929.01	926.66	923.52	$\nu_{24} + \nu_{16} + \nu_{13}$
		1037.50	953.47	943.74	940.38	938.09	938.38	929.92	$\nu_8 + \nu_{48}$
		1039.33	955.68	946.33	941.79	940.70	939.15	937.48	$2\nu_{28}$
		1042.58	958.24	947.33	944.71	944.30	940.14	938.90	$\nu_{10} + 3\nu_{13}$
		1044.60	960.48	955.11	952.53	946.36	943.95	942.02	$\nu_8 + \nu_{13}$
952	940	1045.75	962.95	959.53	954.24	949.54	947.47	942.92	ν_{14}
		1047.45	965.03	963.03	956.78	950.90	950.12	944.11	$\nu_{27} + \nu_{48}$
936	935	1051.07	966.42	965.46	960.51	952.32	950.82	948.87	ν_{43}
		1054.70	968.35	968.07	962.08	957.56	952.14	949.34	$\nu_{47} + \nu_{28}$
		1059.99	975.51	968.47	963.07	958.38	957.28	954.50	$2\nu_{16} + \nu_{48}$
		1062.93	976.31	971.38	968.93	960.17	959.39	957.00	$\nu_{27} + \nu_{13}$
		1065.85	979.37	972.96	970.05	963.84	962.79	961.23	$2\nu_{47}$
		1068.97	984.91	978.18	971.91	967.18	965.92	964.29	$\nu_{36} + 2\nu_{48}$
		1076.05	991.34	984.48	973.41	969.55	969.74	966.39	$2\nu_{16} + \nu_{13}$
		1076.40	1002.54	987.91	981.24	972.97	972.52	967.12	$\nu_{12} + 2\nu_{48}$
		1085.68	1004.96	990.53	986.07	978.64	974.52	968.11	$\nu_{23} + \nu_{48}$

Table 4: (continued)

Exp	VPT2	HI-RRBPM							Assignment
		A	B	C	D	E	F	G	
		1087.59	1008.86	995.36	987.24	983.67	978.48	973.55	$\nu_{36}+\nu_{13}+\nu_{48}$
		1091.20	1010.69	999.37	990.30	984.66	979.84	974.99	$\nu_{23}+\nu_{13}$
		1094.62	1012.71	1000.82	992.98	989.41	982.81	978.30	$\nu_{44}+\nu_{28}$
		1098.74	1017.65	1002.92	996.85	989.96	985.54	981.31	$\nu_{0}+\nu_{28}$
		1099.87	1019.63	1004.24	999.28	993.87	988.08	982.87	$\nu_{36}+\nu_{24}$
		1100.56	1024.01	1010.11	1005.53	994.87	989.53	985.06	$\nu_{24}+\nu_{12}$
		1106.07	1027.30	1011.63	1006.34	997.17	991.32	987.92	$\nu_{44}+\nu_{47}$
		1114.30	1028.04	1015.22	1007.45	999.07	994.09	988.11	$\nu_{12}+\nu_{13}+\nu_{48}$
		1116.75	1030.10	1017.54	1010.37	1001.11	994.78	989.75	$\nu_{36}+2\nu_{13}$
		1120.48	1032.95	1018.27	1010.79	1005.22	998.22	992.29	$\nu_{24}+\nu_{28}+\nu_{48}$
		1121.57	1035.10	1021.70	1014.31	1006.42	1001.41	994.66	$\nu_{0}+\nu_{47}$
		1128.64	1036.63	1027.23	1017.63	1010.96	1004.72	998.71	$\nu_{12}+2\nu_{13}$
		1129.00	1039.04	1029.27	1021.93	1013.51	1006.60	1002.84	$\nu_{24}+\nu_{28}+\nu_{13}$
1011.89[b]	1012	1134.08	1043.80	1033.15	1024.34	1018.20	1015.26	1011.99	ν_{35}
		1138.09	1045.04	1034.98	1027.23	1020.67	1017.14	1013.55	$\nu_{36}+\nu_{16}$
		1138.46	1051.05	1037.28	1030.66	1025.05	1021.81	1015.09	$2\nu_{44}$
		1148.79	1055.63	1040.79	1032.37	1030.58	1024.40	1018.96	$\nu_{0}+\nu_{44}$
		1159.83	1057.70	1042.66	1036.11	1032.25	1026.04	1024.74	$2\nu_{0}$
		1164.45	1066.96	1054.88	1040.33	1033.17	1028.55	1026.52	$\nu_{12}+\nu_{16}$

[a] Ref. 74

[b] Ref. 76

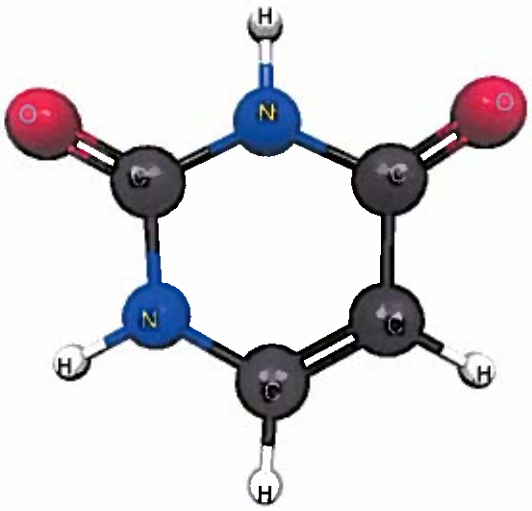

Figure 1: Uracil

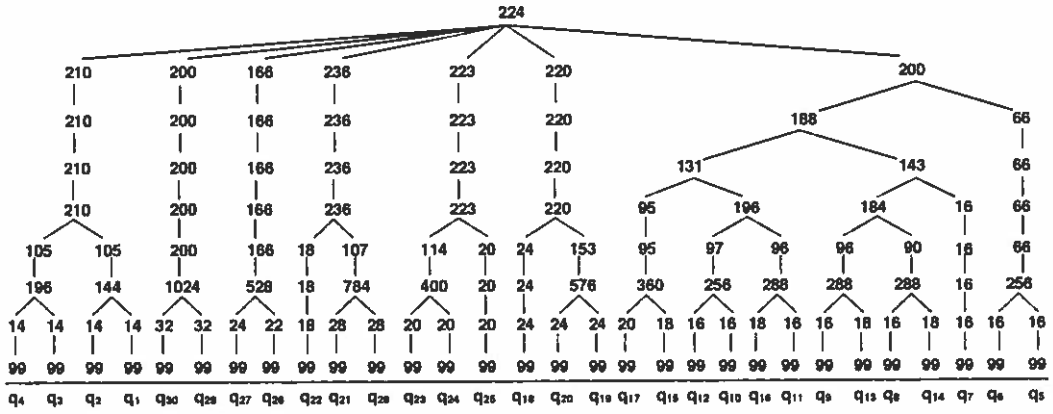

Figure 2: Tree used in calculations on uracil. Numbers appearing at vertices are basis sizes; placement of the primitive coordinates in the leaf nodes is shown at the bottom of the tree.

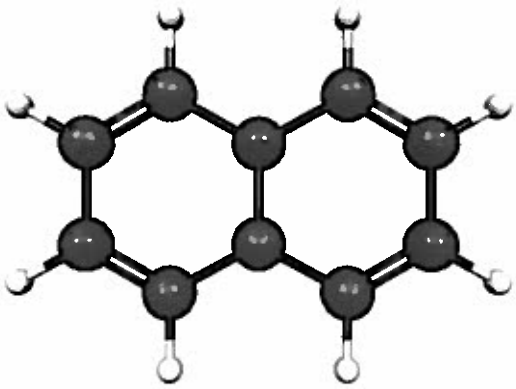

Figure 3: Naphthalene

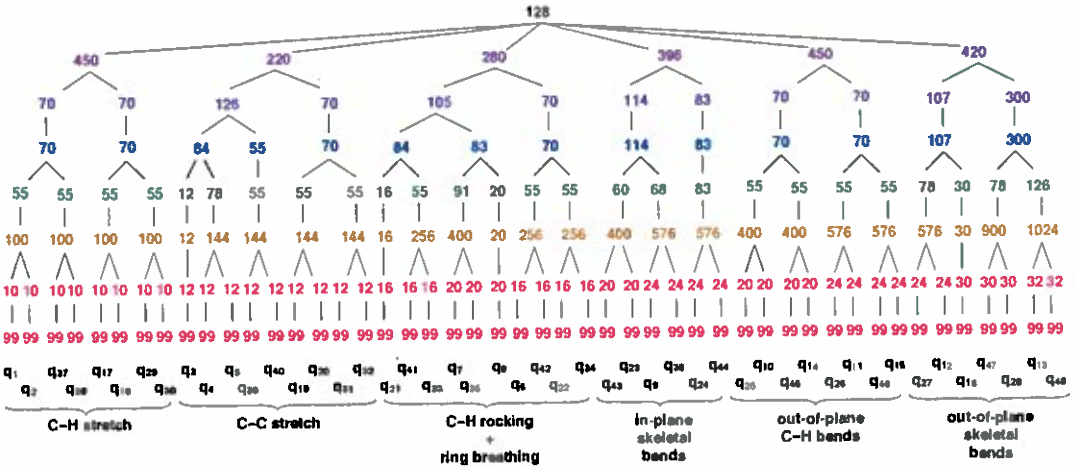

Figure 4: Tree used in calculations on naphthalene. Numbers appearing at vertices are basis sizes; placement of the primitive coordinates in the leaf nodes is shown at the bottom of the tree.